Applied Journal of Physical Science
Volume 7(2), pages 59-71, April 2026
Article Number: 0E4F2F753
ISSN: 2756-6684
https://doi.org/10.31248/AJPS2026.141
https://integrityresjournals.org/journal/AJPS
Full Length Research

# Hankel-based optimization of electromagnetohydrodynamic (EMHD) fluid flow over a cylindrical surface for advanced material processing

**Ojo Adetoye Solomon[1]* and Nwabuzor Peter Onyelukachukwu[2]**

[1]Department of Physics, University of Port Harcourt, PMB 5323 Choba, Nigeria.
[2]Department of Physics with Electronics, University of Port Harcourt, PMB 5323 Choba, Nigeria.

*Corresponding author. Email: solomontoye10@gmail.com; Co-author: peter.nwabuzor@uniport.edu.ng



Received Date: 28 March 2026 | Accepted Date: 24 April 2026 | Published Date: 30 April 2026

**ABSTRACT:** This study presents a Hankel-transform-based analytical framework for optimising electromagnetohydrodynamic (EMHD) fluid flow over a cylindrical surface, motivated by advanced material-processing applications such as coating, extrusion, thermal treatment, and surface modification. The interaction between electromagnetic forces and conductive fluid motion in cylindrical geometries introduces strong radial coupling effects that significantly influence momentum and thermal transport characteristics. To accurately capture these effects, the governing axisymmetric momentum and energy equations are formulated in cylindrical coordinates and solved using the zero-order Hankel transform technique. The transform approach reduces the coupled partial differential equations into algebraic forms in the spectral domain, enabling closed-form analytical solutions for velocity and temperature distributions in terms of Bessel functions. The influence of key nondimensional parameters—including the electromagnetic interaction parameter, Prandtl number, Schmidt number, and thermal radiation parameter is systematically analysed. Results show that electromagnetic forcing enhances flow control capability by modifying boundary layer thickness, while thermal radiation significantly alters radial heat penetration depth. An optimization analysis is conducted to determine parameter regimes that maximize thermal uniformity and minimize hydrodynamic resistance on the cylindrical surface. The Hankel-based spectral formulation provides improved mathematical stability and computational efficiency compared to purely numerical approaches. The findings offer practical design guidelines for EMHD-assisted cylindrical processing systems, contributing to enhanced precision, energy efficiency, and material quality in advanced manufacturing technologies.

**Keywords:** Bessel-function solutions, electromagnetohydrodynamic, exponentially stretching cylinder, Hankel-based optimisation, heat transfer.

## INTRODUCTION

Electromagnetohydrodynamic (EMHD) fluid flow, which arises from the interaction of electrically conducting fluids with simultaneous electric and magnetic fields, has become a central topic in modern transport phenomena due to its wide applicability in advanced manufacturing and thermal engineering systems. Unlike conventional hydrodynamic control mechanisms, EMHD enables direct manipulation of momentum and heat transfer through Lorentz forces, thereby offering a non-invasive and highly responsive means of regulating boundary-layer behaviour. This capability is particularly significant in cylindrical configurations commonly encountered in industrial processes such as fibre coating, polymer extrusion, thermal annealing, and surface deposition, where curvature effects strongly influence flow stability and heat distribution.

The modelling of EMHD flows over curved geometries introduces substantial analytical complexity. The governing equations in cylindrical coordinates inherently involve radial coupling and singular behaviour, making

direct analytical treatment challenging. Consequently, earlier studies have largely relied on numerical or semi-analytical techniques to examine magnetohydrodynamic (MHD) and EMHD transport characteristics. For instance, Preetham and Kumbinarasaiah (2024) demonstrated that numerical collocation techniques provide accurate and stable solutions for MHD boundary-layer flow over exponentially stretching sheets with heat absorption, generation, and chemical reaction effects. Similarly, Kayalvizhi and Vijaya Kumar (2022) analysed entropy generation in EMHD hybrid nanofluid systems, revealing the strong dependence of thermal efficiency on radiation and porous medium effects.

Recent investigations into hybrid nanofluid and curved surface flows further highlight the sensitivity of velocity and temperature distributions to electromagnetic forcing and thermal conditions. Studies such as those by Sandeep *et al*. (2025) and Muhammad *et al*. (2024) emphasise that magnetic field orientation, radiation intensity, and surface stretching significantly alter boundary-layer thickness and heat transfer rates. Complementary research by Abbas *et al*. (2023) demonstrated that convective boundary conditions, viscous dissipation, and magnetic field effects significantly influence the thermal behaviour and flow characteristics of MHD fluid systems over stretching surfaces.

Building on these developments, earlier contributions by Adetoye *et al*. (2025) have provided valuable insight into cylindrical nanofluid dynamics. In particular, their analytical investigation of silver nanofluid flow over cylindrical enclosures established the influence of magnetic fields, thermal conductivity models, and viscosity variations on velocity, temperature, and concentration distributions. These findings were further complemented by numerical studies incorporating Laplace transform techniques and non-dimensional analysis, which revealed the intricate coupling between Lorentz forces, conductive properties, and convective transport mechanisms (Nascimento *et al*., 2024). Such studies underscore the strong linkage between classical MHD and EMHD frameworks, suggesting that the inclusion of electric field effects can further enhance flow controllability and thermal regulation.

The increasing demand for precision in industrial processes has intensified the need for advanced flow control strategies. Applications such as thin-film coating, continuous casting, and glass fibre production involve stretching or moving cylindrical surfaces that generate nonlinear velocity fields and complex thermal gradients. In these systems, even minor variations in boundary-layer characteristics can significantly affect surface quality, structural integrity, and energy efficiency. MHD-based flow control offers a promising pathway to address these challenges by enabling precise regulation of fluid motion and thermal transport, thereby improving thermal efficiency and enhancing the uniformity of transport processes (Mburua *et al*., 2024).

Heat transfer mechanisms within EMHD boundary layers are equally critical, particularly under high-temperature operating conditions. Thermal radiation can substantially enhance heat transport, while Joule heating resulting from electrical current dissipation can either improve thermal energy distribution or lead to localised overheating if not properly managed. Recent investigations by Khader *et al*. (2023) revealed that spectral collocation techniques are highly effective for handling the nonlinear and stiff nature of governing equations in MHD transport problems. Fourier pseudospectral methods and reduced-order modelling approaches have demonstrated superior convergence, computational efficiency, and accuracy compared to traditional numerical schemes (Albuquerque *et al*., 2024; Nascimento *et al*., 2024). These methods allow compact representation of spatial variations and enable efficient parametric analysis of key dimensionless quantities such as Hartmann number, Prandtl number, and radiation parameter. Furthermore, spectral optimisation frameworks have proven effective in identifying optimal electromagnetic configurations that achieve desired thermal and hydrodynamic performance (Muzara and Shateyi, 2023).

Despite these advances, most existing studies rely predominantly on Fourier-based or numerical approaches, with limited attention given to transform methods specifically suited to cylindrical geometries. In particular, the application of Hankel transform techniques—which naturally incorporate Bessel function representations and radial symmetry—remains underexplored in the context of EMHD flow optimisation. Given the inherent compatibility of Hankel transforms with cylindrical domains, their use offers significant potential for deriving closed-form analytical solutions and gaining deeper physical insight into radial transport phenomena.

Motivated by this gap, the present study develops a Hankel-transform-based analytical framework for the investigation and optimisation of EMHD fluid flow over a cylindrical surface. By transforming the governing equations into the spectral domain, the approach yields tractable solutions for velocity and temperature fields while preserving the essential physics of electromagnetic coupling and curvature effects. This formulation not only enhances mathematical tractability but also provides a robust basis for optimising process parameters in advanced material processing applications. Ultimately, the study contributes to both theoretical advancements in EMHD modelling and practical improvements in industrial system design, where precise control of flow and heat transfer is essential for achieving high-quality manufacturing outcomes.

## MATHEMATICAL FORMULATION OF THE PROBLEM

The continuity equation, momentum equation, the energy equation and the equation of concentration are the main

partial differential equations that theoretically validate the impacts of chemical reactions and radiation, respectively.

$$\frac{\partial \rho}{\partial t} + \frac{\partial ur}{\partial r} = 0 \quad (1)$$

$$\rho \frac{\partial u_{(r)}}{\partial t} = -\nabla \rho + \mu \nabla^2 u + g\beta_\theta(\theta - \theta_*) + g\beta_\phi(\phi - \phi_*) - \sigma B_0^2 u_r - \sigma_0 \quad (2)$$

$$\left(\rho C_p\right)\frac{\partial \theta_{(r)}}{\partial r} = K\frac{\partial^2 \theta}{\partial r^2} - \frac{\partial}{\partial r}\left(q_{(r)}\right) \quad (3)$$

$$\left(\rho C_p\right)\frac{\partial \phi}{\partial r} = D\frac{\partial^2 \phi}{\partial r^2} - K_0^2 \phi \quad (4)$$

In a situation where (EMHD) fluid flow is considered incompressible, and is subjected to a steady state flow condition in the Cartesian system, then equations (2) – (4), with the use of equation (1), are transformed into

$$\frac{1}{\rho}\mu\nabla^2 u - \frac{1}{\rho}\nabla\rho + \frac{g\beta_\theta(\theta-\theta_*)}{\rho} + \frac{g\beta_\phi(\phi-\phi_*)}{\rho} - \frac{\sigma B_0^2 u_r}{\rho} - \frac{\sigma_0}{u_r} = 0 \quad (5)$$

$$\frac{1}{(\rho C_p)}K\frac{\partial^2 \theta}{\partial r^2} - \frac{1}{(\rho C_p)}\frac{\partial}{\partial r}\left(q_{(r)}\right) = 0 \quad (6)$$

$$\frac{1}{(\rho C_p)}D\frac{\partial^2 \phi}{\partial r^2} - \frac{1}{(\rho C_p)}K_0^2\phi = 0 \quad (7)$$

Where: u = fluid velocity, $\theta$ = temperature, $\rho$ = fluid density, $\mu$ = viscosity of fluid, $C_p$ = specific heat at persistent pressure, $q_r$= radiation term, K = thermal conductivity of fluid, $K_0$ = chemical reaction term, D = chemical molecular diffusivity, $\phi$ = fluid concentration.

By using Rosseland approximation ($q_r$) to consider the effect of radiation on an optically thick model in which the thermal layer becomes very thick.

$$q_{(r)} = -\frac{1}{3\alpha}4K_B\frac{\partial}{\partial r}\theta^4 \quad (8)$$

Where: $K_B$ is the Stefan-Boltzmann constant, and $\alpha$ is the absorption coefficient. It is assumed that the temperature difference within the flow is sufficiently small such that $\theta^4$ can be expressed as a linear function of temperature. This is accomplished by expanding $\theta^4$ in a Taylor series about $\theta_\infty$ and neglecting higher order terms, the expression results in to

$$\theta^4 = 4\theta_\infty^3\theta - 3\theta_\infty^4 \quad (9)$$

Using equations (8) and (9), equation (6) takes the form

$$\frac{\rho}{r}\frac{\partial \theta}{\partial r} = \frac{1}{(\rho\hat{C_p})}K\left(1 + \frac{16K_0\theta^3}{3\alpha}\right)\frac{1}{r}\frac{\partial}{\partial r}\left(r\frac{\partial \theta}{\partial r}\right) - \frac{1}{(\rho\hat{C_p})}K\frac{1}{r}q_{(r)} \quad (10)$$

**Dimensional analysis**

Equations 5-7 are transformed into dimensionless parameters of the Schmidts number, Prandtls number, Grashof number, Radiation parameter, Heat function, Electroconductivity and Magnetic term. The dimensionless quantities used are:

$$Re^{-1} = \frac{\mu\rho}{\rho\mu}, Pr = \frac{k(\rho Cp)}{k(\rho C_p)}, Sc = \frac{k(\rho C_p)}{D(\rho C_p)}, u = \frac{v_r t^*}{r}, r = \frac{r^*}{d}, k_0 = \frac{k_r^2(\rho C_p)}{(\rho C_p)v^{*2}}, Gr_\theta = \frac{g\beta(\theta-\theta_0)\mu}{{v_r}^2\beta}, Gr_\phi = \frac{g\beta^*(\phi-\phi_0)\mu}{{v_r}^2\beta^*}, \theta = \frac{\theta-\theta_0}{\theta_0}, \phi = \frac{\phi-\phi_0}{\phi_0}, \Re = \frac{16\zeta\theta_0^3\rho}{3\alpha(C_p)}, H_a = \frac{\sigma {B_0}^2 v_r}{\rho}, \sigma_0 = \frac{\sigma_0}{v_r}$$

Rewriting equations (5), (7) and (10) in dimensionless form, the modelled equations are transformed into

$$\frac{1}{Re}\left[\frac{1}{r}\frac{\partial u_r}{\partial r} + \frac{\partial^2 u_r}{\partial r^2}\right] - \frac{1}{r}\frac{\partial u_r}{\partial r} + Gr_\theta\theta + Gr_\phi\phi - H_a u_r - \sigma_0 u_r = 0 \quad (11)$$

$$\frac{1}{Pr}\left[\frac{1}{r}\frac{\partial \theta}{\partial r} + \frac{\partial^2 \theta}{\partial r^2}\right] - \frac{1}{r}\frac{\partial \theta}{\partial r} - \Re\left(\frac{1}{r}\frac{\partial \theta}{\partial r} + \frac{\partial^2 \theta}{\partial r^2}\right) = 0 \quad (12)$$

$$\frac{1}{Sc}\left[\frac{1}{r}\frac{\partial \phi}{\partial r} + \frac{\partial^2 \phi}{\partial r^2}\right] - \frac{1}{r}\frac{\partial \phi}{\partial r} - \frac{1}{r}K_0\phi = 0 \quad 13)$$

Where: Re = Reynolds number, Pr = Prandlt number, Sc = Schmidt number, $G_{r_\theta}\theta$ = thermal Grashofs number, $G_{r_\phi}\phi$ = modified Grashofs number, $\Re$ = dimensionless radiation term, $\theta$ = dimensionless temperature, u = dimensionless velocity, $\phi$ = dimensionless concentration, $H_a$ = magnetic Hartmann number, $\sigma_0$ = electroconductivity term $k_0$ = dimensionless chemical reaction term and r = dimensionless area of fluid flow.

**Solution technique**

We consider the steady, laminar flow of an incompressible, electrically conducting fluid over an exponentially stretching cylindrical surface. Equation (13) can be rewritten as

$$\frac{1}{Sc}\nabla_r^2\phi - \frac{1}{r}\frac{\partial \phi}{\partial r} - \frac{K_0}{r}\phi = 0 \quad (14)$$

Where $\nabla_r^2\phi = \phi_{rr} + \frac{1}{r}\phi_r$ (15)

Multiply equation (14) by Sc

$$\nabla_r^2\phi - Sc\frac{1}{r}\frac{\partial \phi}{\partial r} - Sc\frac{K_0}{r}\phi = 0 \quad (16)$$

Apply the Zero-order Hankel transform

$$\tilde{\phi}(k) = \int_0^\infty \phi(r)J_0(kr)rdr \quad (17)$$

Applying the Hankel transform into (16), it gives

$$H_0[\nabla_r^2\phi] = -k^2\tilde{\phi}(k) \quad (18)$$

Equation (16) is transformed to

$$H_0[\nabla_r^2\phi] = -k^2\tilde{\phi}(k),\ H_0\left[\frac{1}{r}\frac{\partial\phi}{\partial r}\right] = -k\tilde{\phi}(k) \quad (19)$$

Also, for the $-\frac{K_0}{r}\phi$ term, Hankel transform gives approximately $-K_0\tilde{\phi}(k)$ in eigenvalue form.

Applying Hankel transform equation (14) becomes

$$\frac{1}{Sc}\left(-k^2\tilde{\phi}\right) - \left(-k\tilde{\phi}\right) - k_0\tilde{\phi} = 0 \quad (20)$$

$$-\frac{k^2}{Sc}\tilde{\phi} + k\tilde{\phi} - k_0\tilde{\phi} = 0 \quad (21)$$

$$\tilde{\phi} = \left(-\frac{k^2}{Sc} + k - k_0\right) = 0 \quad (22)$$

Equation (21) is a non-trivial solution in the form of a quadratic in k:

$$-\frac{k^2}{Sc} + k - k_0 = 0 \Rightarrow k^2 - Sck + Sck_0 = 0 \quad (23)$$

Using quadratic formula to solve equation (23)

$$k = \frac{Sc \pm \sqrt{Sc^2 - 4Sck_0}}{2} = \frac{Sc \pm \sqrt{Sc(Sc-4k_0)}}{2} \quad (24)$$

Applying Inverse Hankel Transform with discrete eigenvalues solution gives

$$\phi(r) = C_1 + C_2J_0(kr) \quad (25)$$

Substitute equation (24) into (25) it yields

$$\phi(r) = C_1 + C_2J_0\left(\frac{Sc+\sqrt{Sc(Sc-4k_0)}}{2}r\right) + C_3J_0\left(\frac{Sc-\sqrt{Sc(Sc-4k_0)}}{2}r\right) \quad (26)$$

Boundary conditions

- At $r = 0$: regularity → finite, automatically satisfied since $J_0(0) = 1$
- At $r = a$: wall concentration $\phi(a) = \phi_w$→ solve for $C_1, C_2, C_3$
- At $r \to \infty$: for bounded solution, discard divergent terms (if $k$is complex with growing exponential)

Final Concentration Solution using Hankel Method in the form of a standard modified Bessel equation of order zero.:

$$\phi(r) = AI_0(\lambda r) + BK_0(\lambda r) \quad (27)$$

where: $\lambda^2 = Sc\,K_0$

The radial Laplacian form of equation (12) gives

$$\nabla_r^2\theta = \theta_{rr} + \frac{1}{r}\theta_r \quad (28)$$

Substituting equation (28) into (12), it becomes

$$\left(\frac{1}{Pr} - R\right)\nabla_r^2\theta - \frac{1}{r}\theta_r = 0 \quad (29)$$

Let $A = \left(\frac{1}{Pr} - R\right)$

Then equation (29) becomes

$$A\nabla_r^2\theta - \frac{1}{r}\theta_r = 0 \quad (30)$$

Apply Zero-Order Hankel Transform

$$\tilde{\theta}(k) = \int_0^\infty \theta(r)J_0(kr)rdr \quad (31)$$

Key properties of the Hankel Transform give

$$H_0[\nabla_r^2\theta] = -k^2\tilde{\theta}(k)$$

$$H_0\left[\frac{1}{r}\theta_r\right] = -k\tilde{\theta}(k) \quad (32)$$

Applying equation (32) term-by-term it implies

$$A\left(-k^2\tilde{\theta}\right) - \left(-k\tilde{\theta}\right) = 0 \quad (33)$$

$$\tilde{\theta}(k)(-Ak^2 + k) = 0 \quad (34)$$

Solving equations (33) and (34) in the inverse Hankel Transform

$$\theta(r) = \int_0^\infty \tilde{\theta}(k)J_0(kr)dk \quad (35)$$

Since the solution exists only at discrete eigenvalues, we obtain:

$$\theta(r) = C_1 + C_2J_0\left(\frac{r}{A}\right) \quad (36)$$

Where $A = \frac{1}{Pr}$

Boundary Conditions (Cylindrical)

Regularity at centre r = 0 since $J_0(0) = 1$, solution remains finite automatically.

For a finite cylinder $0 \le r \le a$, wall temperature condition: $\theta(a) = \theta_w$, then:

$$C_1 + C_2J_0\left(\frac{a}{A}\right) = \theta_w$$

For the exterior region, $\boldsymbol{r} \to \infty$

Because $J_0$ oscillates does not decay, boundedness requires: $C_2 = 0$

Solution of the temperature equation obtained using the Zero-Order Hankel Transform in Cylindrical coordinates becomes:

$$\theta(r) = C_1 + C_2 J_0\left(\frac{r}{\frac{1}{Pr} - R}\right) \quad (37)$$

Equation (11) can be written in cylindrical Laplacian form

$$\frac{1}{Re}\nabla_r^2 u - \frac{1}{r}u + Gr_\theta\theta + Gr_\phi\phi - (H_a + \sigma_0)u = 0 \quad (38)$$

Let equations (27) and (37) become

$$\theta(r) = A_1 + A_2 J_0(\lambda_T r) \quad (39)$$

$$\phi(r) = B_1 + B_2 J_0(\lambda_C r) \quad (40)$$

Substitute equations (39) and (40) into the momentum equation (38)

$$\frac{1}{Re}\nabla_r^2 u\frac{1}{r}(H_a + \sigma_0)u + Gr_\theta\theta\left(A_1 + A_2 J_0(\lambda_T\gamma)\right) + Gr_\phi\phi\left(B_1 + B_2 J_0(\lambda_C\gamma)\right) \quad (41)$$

Apply Zero-Order Hankel Transform

$$\tilde{u}(k) = \int_0^\infty u(r) J_0(kr) r dr \quad (42)$$

Key properties of the Hankel Transform give

$$H_0[\nabla_r^2 u] = -k^2\tilde{u}$$

$$H_0\left[\frac{1}{r}u\right] - k\tilde{u} \quad (43)$$

Transform each term in equation (41)

Laplacian term: $\frac{1}{Re(-k^2\tilde{u})}$

Second term: $-(-k\tilde{u}) = +k\tilde{u}$

Velocity damping: $-(H_a + \sigma_0)\tilde{u}$

Let Hankel transform of $J_0(\lambda r)$gives delta function:

$$H_0[J_0(\lambda r)] = \frac{1}{k}\delta(k - \lambda) \quad (44)$$

Constants produce $\delta(k)$, equation (41) becomes

$$\left[-\frac{k^2}{Re} + k - (H_a + \sigma_0)\right]\tilde{u} = -Gr_\theta\tilde{\theta} - Gr_\phi\tilde{\phi} \quad (45)$$

$$\tilde{u}(k) = \frac{Gr_\theta\tilde{\theta}(k) + Gr_\phi\tilde{\phi}(k)}{\frac{k^2}{Re} - k + (H_a + \sigma_0)} \quad (46)$$

Apply Inverse Hankel Transform

$$v(r) = \int_0^\infty \tilde{u}(k) J_0(kr) k dk \quad (47)$$

Let $k = \lambda_T, k = \lambda_C$final velocity solution become

$$u(r) = C_0 + \frac{Gr_\theta A_2}{D(\lambda_T)}J_0(\lambda_T r) + \frac{Gr_\phi B_2}{D(\lambda_C)}J_0(\lambda_C r) \quad (48)$$

where: $D(k) = \frac{k^2}{Re(H_a + \sigma_0)}$

Applying boundary conditions (Cylindrical Flow)

For a solid cylinder $0 \le r \le a$:

$$v \text{ finite at } r = 0, J_0(0) = 1, v(a) = 0, \frac{dv}{dr}(0) = 0, J_0'(0) = 0 \quad (49)$$

Final compact solution for momentum equation

$$u(r) = C_0 + \frac{Gr_\theta A_2}{\frac{\lambda_T^2}{Re} - \lambda_T + (H_a + \sigma_0)}J_0(\lambda_T r) + \frac{Gr_\phi B_2}{\frac{\lambda_C^2}{Re} - \lambda_C + (H_a + \sigma_0)}J_0(\lambda_C r) \quad (50)$$

**Optimisation and application of electromagnetohydrodynamic fluid flow**

Optimisation of electromagnetohydrodynamic (EMHD) fluid flow plays a critical role in enhancing heat and mass transfer in electrically conducting fluids through the effective control of key governing parameters, including magnetic field intensity and thermal radiation effects. In the present study, the Fourier transform method is employed to obtain analytical solutions, enabling clear identification of optimal conditions for improved transport performance. Optimised EMHD flow systems have wide-ranging applications in engineering and technology, including electromagnetic pumping, advanced cooling systems, metallurgical processing, and microfluidic devices, where precise control of fluid motion and thermal characteristics is essential. The analysis reveals that optimal system performance can be achieved under appropriate combinations of governing parameters, as outlined below:

***Effective thermal diffusivity***

The effective thermal diffusivity represents the modified capacity of the fluid to conduct and diffuse heat in the presence of additional physical effects, particularly thermal radiation. It accounts for the combined contribution of classical molecular heat conduction and radiative heat transfer within the fluid medium. This parameter plays a key role in governing the rate at which temperature variations propagate through the boundary layer and, consequently, strongly influences the overall heat transfer characteristics of the system. Mathematically, the effective thermal diffusivity is expressed as:

$$\alpha_{eff} = \alpha\left(1 + \frac{4}{3}R\right) \quad (51)$$

Where the radiation parameter R is

$$R = \frac{4\sigma^* T_\infty^3}{kk^*} \quad (52)$$

### *Sherwood number*

This parameter represents the rate of mass transfer from the stretching surface into the surrounding fluid. It is a dimensionless quantity that characterises the relative dominance of convective mass transport over molecular diffusion within the boundary layer. A higher Sherwood number corresponds to enhanced mass transfer rates and a thinner concentration boundary layer in the vicinity of the surface.

$$Sh = -\frac{d\phi}{dr}\Big|_{r=0} = \lambda = \sqrt{ScK_0} \quad (53)$$

### *Nusselt number*

The Nusselt number $(Nu)$ characterises the rate of heat transfer from the stretching surface to the adjacent fluid within the boundary layer. It is a dimensionless parameter that represents the ratio of convective heat transfer to conductive heat transfer at the surface. In electromagnetohydrodynamic (EMHD) flow over an exponentially stretching sheet, the Nusselt number indicates the effectiveness of thermal energy transport from the surface into the electrically conducting fluid. A higher Nusselt number signifies enhanced heat transfer at the surface, leading to a thinner thermal boundary layer and more efficient heat removal from the stretching sheet.

$$Nu = \sqrt{\frac{Pr\,\lambda}{1+\frac{4}{3}R}} \quad (54)$$

### *Skin friction coefficient*

The skin friction coefficient is a dimensionless parameter that quantifies the shear stress exerted by the fluid on the stretching surface due to its motion. It represents the resistance offered by the fluid to the movement of the surface and is directly related to the velocity gradient at the wall. In electromagnetohydrodynamic (EMHD) flow, the skin friction coefficient provides insight into the influence of the magnetic field, boundary forces, and other governing parameters on the near-wall flow behaviour. A higher value of the skin friction coefficient indicates increased frictional drag between the fluid and the stretching sheet.

$$C_f = \frac{du}{dr}\Big|_{r=0} \quad (55)$$

Differentiating the velocity solution gives

$$C_f = \frac{Gr_\theta}{M-\beta^2}\left(-\frac{1}{2}+\frac{\beta}{2\sqrt{M}}\right) + \frac{Gr_\phi}{M-\lambda^2}\left(-\frac{1}{2}+\frac{\lambda}{2\sqrt{M}}\right) \quad (56)$$

### Entropy generation analysis

Entropy generation represents the thermodynamic irreversibility occurring within the fluid system. It quantifies the rate of energy degradation resulting from heat transfer, viscous dissipation, magnetic effects, and mass diffusion. Through entropy generation analysis, it becomes possible to identify the dominant mechanisms responsible for energy loss and system inefficiency. This analysis is particularly important in electromagnetohydrodynamic (EMHD) flows, as it provides a basis for optimising operating conditions that enhance heat and mass transfer while minimising irreversibility, thereby improving overall thermal-fluid performance. The dimensional local entropy generation rate is expressed as follows:

$$S_{gen}^{!!!} = \frac{k}{T_\infty^2}\left(\frac{\partial\theta}{\partial r}\right)^2 + \frac{\mu}{T_\infty}\left(\frac{\partial u}{\partial r}\right)^2 + \frac{\sigma B_0^2}{T_\infty}u^2 + \frac{D}{T_\infty}\left(\frac{\partial\phi}{\partial r}\right)^2 \quad (57)$$

Applying dimensionless analysis on equation (66) it becomes the entropy generation number

$$N_s = \left(\frac{\partial\theta}{\partial r}\right)^2 + Br\left(\frac{\partial u}{\partial r}\right)^2 + Mu^2 + \Gamma\left(\frac{\partial\phi}{\partial r}\right)^2 \quad 58)$$

### Exact Solutions

Exact solutions refer to closed-form analytical expressions for the velocity, temperature, and concentration fields that exactly satisfy the governing differential equations together with the associated boundary conditions. These solutions provide valuable physical insight into the influence of key flow parameters on the system behaviour. In addition, they enable the precise evaluation of important engineering quantities such as the Nusselt number, Sherwood number, and skin friction coefficient.

Recall

$$\theta = e^{-\beta r} \quad (59)$$

$$\phi = e^{-\lambda r} \quad (60)$$

$v(r)$ =(sum of exponential terms)

Solve the first derivative of equations (59) and (60)

$$\frac{\partial\theta}{\partial r} = -\beta e^{-\beta r} \quad (61)$$

$$\frac{\partial\phi}{\partial r} = -\lambda e^{-\lambda r} \quad (62)$$

Solve the second derivative of equations (61) and (62)

$$\left(\frac{\partial\theta}{\partial r}\right)^2 = \beta^2 e^{-2\beta r} \quad (63)$$

$$\left(\frac{\partial\phi}{\partial r}\right)^2 = \lambda^2 e^{-2\lambda r} \quad (64)$$

**Table 1.** Selected realistic values of dimensionless hydrodynamic parameters

| Parameters | Value |
|---|---|
| Prandtl number (Pr) | 3.5, 7.0, 10.5, 14.0, 17.5 |
| Reynolds number (Re) | 10, 20, 30, 40, 50 |
| Schmidt number (Sc) | 2.5, 4.5, 6.5, 8.5, 10.5 |
| Radiation term ($\mathfrak{R}$) | 3.5, 6.5, 9.5, 12.5, 15.5 |
| Grashof number ($Gr_\phi$) due to concentration | 3.2, 6.4, 9.6, 12.8, 16.0 |
| Grashof number ($Gr_\theta$) due to temperature | 2.6, 5.2, 7.8, 10.4, 13.0 |
| Magnetic Hartmann Number (Ha) | 0.5, 1.5, 2.5, 3.5, 4.5 |
| Chemical reaction term (k0) | 1.8, 3.6, 5.4, 7.2, 9.0 |
| Electro-conductivity term ($\sigma_0$) | 0.25, 0.50, 1.75, 1.00, 1.25 |

Substitute equations (63) and (64) into (58), which gives the final entropy generation expression

$$N_s = \beta^2 e^{-2\beta r} + Br\left(\frac{\partial u}{\partial r}\right)^2 + Mu^2 + \Gamma\lambda^2 e^{-2\lambda r} \qquad (65)$$

## RESULTS AND DISCUSSION

For clearer insight into the physical problem and application of electromagnetohydrodynamic (EMHD) fluid flow for advanced material processing equations (27), (37) and (50), together with the modified boundary conditions, are solved numerically with Table 1 using the Zero-Order Hankel Transform Method. The resulting computational fluid dynamics outcomes over a cylindrical surface for advanced material processing are illustrated through the graphs in Figures 1 to 20.

The variation of the concentration profile $\phi$ with the radial coordinate $r$ in cylindrical coordinates for different values of the chemical reaction parameter $k_0$ is shown in Figure 1. This figure presents the variation of concentration $\phi$with radial distance $r$ for different chemical reaction rates $k_0$. It is observed that increasing $k_0$ enhances species consumption, leading to a sharper decay of concentration near the cylindrical surface and a thinner concentration boundary layer. This behaviour is in agreement with the findings of Ahmad *et al.* (2023), who reported that higher chemical reaction parameters significantly reduce species concentration in MHD nanofluid flows due to intensified reactive depletion. Similarly, Alsharif *et al*. (2024) observed that strong chemical reaction effects accelerate mass transfer attenuation, thereby thinning the concentration boundary layer in stretching surface problems.

Figure 2 illustrates the influence of the Schmidt number ($Sc$) on the concentration profile. It is evident that increasing $Sc$reduces molecular diffusivity, resulting in steeper concentration gradients and a thinner boundary layer, whereas lower $Sc$enhances diffusion and allows deeper penetration of species into the fluid domain. This trend aligns with the results of Alatyar *et al*. (2023), who demonstrated that higher Schmidt numbers suppress mass diffusion and significantly reduce solutal boundary-layer thickness in nanofluid transport. Likewise, Hayat *et al*. (2024) confirmed that diffusion-dominated regimes strongly influence concentration decay behaviour in EMHD/MHD flows.

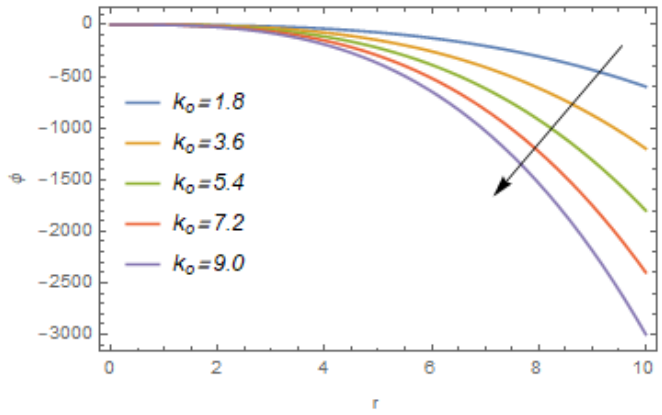


**Figure 1.** Concentration profile $\phi$ against boundary layer r for varying chemical reaction term $k_0$.

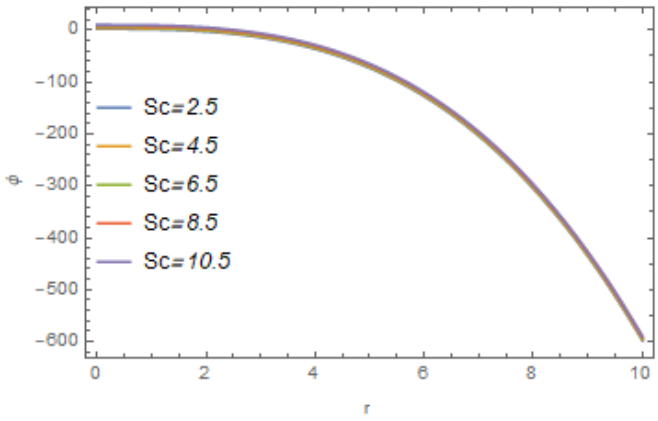


**Figure 2.** Concentration profile $\phi$ against boundary layer r for varying Schmidt number Sc.

Figure 3 presents the temperature distribution for varying radiation parameter values along the radial

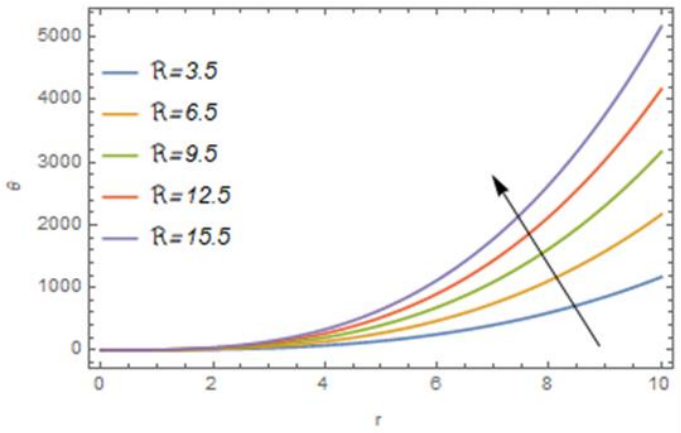


**Figure 3.** Temperature profile $\theta$ against boundary layer r for varying Radiation term $(\Re)$.

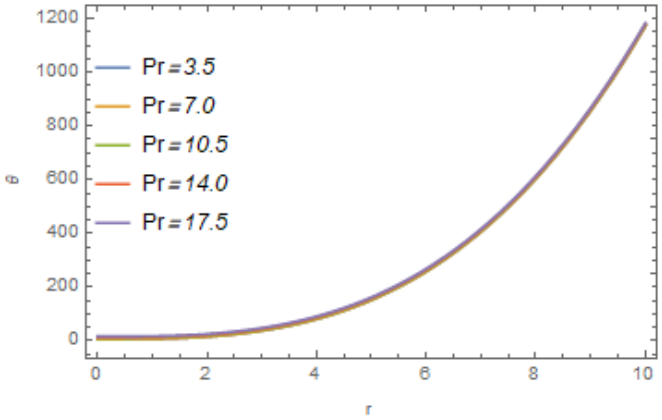


**Figure 4.** Temperature profile $\theta$ against boundary layer r for varying Prandtl number Pr.

direction. Increasing radiation enhances heat transfer, raising temperature levels within the boundary layer. Consequently, the thermal boundary layer becomes thicker due to deeper heat penetration. This outcome is in agreement with the findings of Ojo and Egbo (2025) displaying the lower radiation reduces energy transport, resulting in thinner thermal layers. This demonstrates the strong influence of radiative heat transfer in EMHD systems.

Figure 4 shows the temperature profile for different Prandtl numbers (Pr) along the radial coordinate. Higher Pr reduces thermal diffusivity, leading to steeper temperature gradients and thinner thermal boundary layers. In contrast, lower Pr allows heat to diffuse more easily, producing thicker thermal layers. This behaviour is crucial in regulating heat transfer characteristics. It has direct implications for thermal control in material processing this is in agreement with the results of Adetoye *et al*. (2026).

Figure 5 depicts the velocity distribution for varying

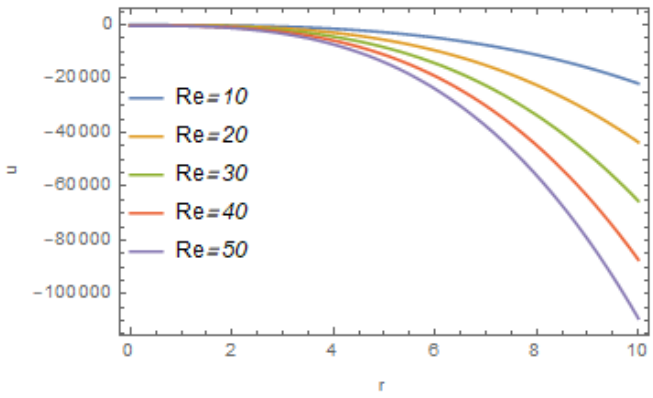


**Figure 5.** Velocity profile u against boundary layer r for varying Reynolds number (Re).

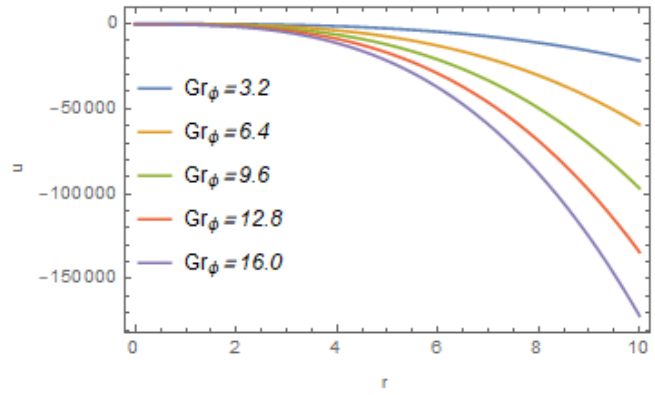


**Figure 6.** Velocity profile u against boundary layer r for varying Grashof number in term of concentration $(Gr_\phi)$.

Reynolds numbers along the radial direction. Higher Reynolds numbers enhance inertial effects, increasing fluid velocity near the surface and thinning the boundary layer. Lower Reynolds numbers strengthen viscous forces, reducing velocity and thickening the boundary layer. The results illustrate the competition between inertia and viscosity. This is essential for understanding flow behaviour in EMHD systems. This outcome is in line with the findings of Ojo *et al*. (2026).

Figure 6 shows the velocity profile for different concentration Grashof numbers $Gr_\phi$. Increasing $Gr_\phi$ strengthens buoyancy forces, resulting in higher velocities and thicker boundary layers. Lower values weaken buoyancy effects, reducing flow intensity. This demonstrates the role of concentration-driven natural convection. The results are important for mass-transfer-driven EMHD flows. This result agreed with the findings of Gupta *et al*. (2025).

Figure 7 shows the influence of chemical reaction parameter $k_0$on the velocity profile. Higher $k_0$reduces species concentration, weakening buoyancy forces and lowering velocity. This leads to a thinner velocity boundary

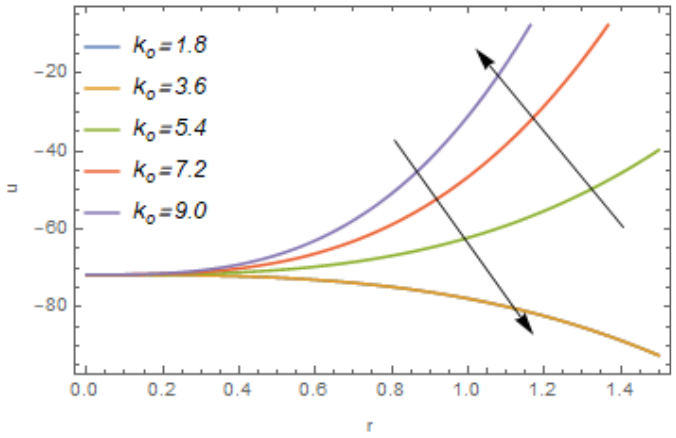


**Figure 7.** Velocity profile u against boundary layer r for varying chemical reaction term $(k_0)$.

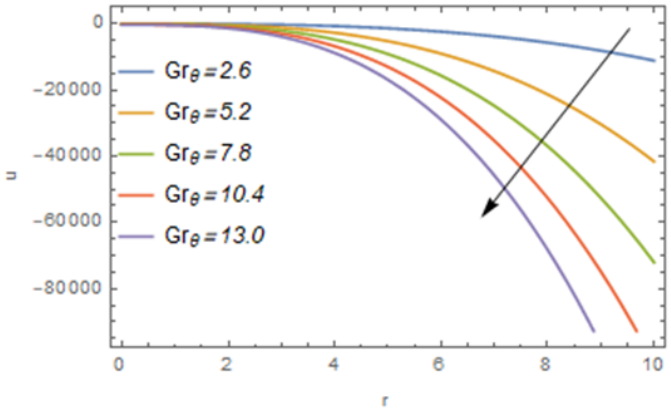


**Figure 9.** Velocity profile u against boundary layer r for varying Grashof number in term of temperature $(Gr_\theta)$.

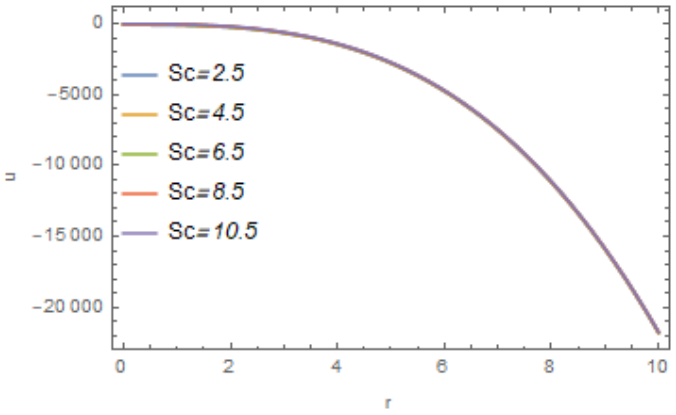


**Figure 8.** Velocity profile u against boundary layer r for varying Schmidt number (Sc).

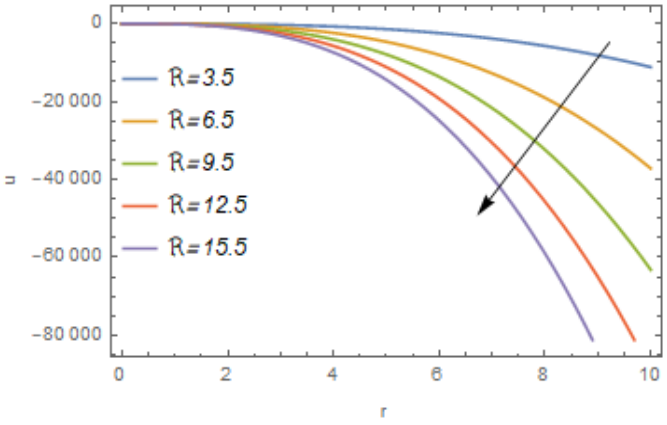


**Figure 10.** Velocity profile u against boundary layer r for varying Radiation term $(\Re)$.

layer. Conversely, smaller $k_0$ enhances concentration and increases flow velocity. This outcome is in agreement with the findings of Aljaloud *et al*. (2025). Their results reveal the coupling between chemical reaction and fluid motion.

Figure 8 displays the velocity profile plotted for varying Schmidt numbers (Sc). Higher Sc reduces species diffusivity, weakening buoyancy-induced flow and lowering velocity. This results in a thinner velocity boundary layer. Lower Sc enhances diffusion, increasing buoyancy effects and velocity magnitude. The figure highlights the interaction between mass diffusion and momentum transport. This is in agreement with the findings of Uda *et al*. (2002).

Figure 9 illustrates the effect of thermal Grashof number $Gr_\theta$on velocity distribution. Increasing $Gr_\theta$enhances temperature-induced buoyancy, raising velocity and thickening the boundary layer. Lower values reduce buoyancy forces and flow strength. This demonstrates the role of thermal convection in EMHD flow. It is significant for heat-driven transport processes in line with the finding of Uda *et al*. (2001).

Figure 10 showcases the velocity profile for different radiation parameters (R). Increasing R enhances radiative heating, which strengthens buoyancy forces and increases velocity. This leads to a thicker velocity boundary layer. Lower R weakens thermal effects, reducing flow intensity. The results emphasise the indirect influence of radiation on fluid motion which proves the exact result with Shin-Ya *et al*. (2006).

Figure 11 presents the velocity profile for varying Prandtl numbers. Higher Pr reduces thermal diffusivity, indirectly influencing momentum transport and reducing velocity spread. Lower Pr enhances thermal diffusion and broadens the velocity profile. This demonstrates the coupling between heat and momentum transfer which also proves the same output with Ojo *et al*. (2025). It is important for optimising coating and thermal processes.

Figure 12 illustrates the effect of the Hartmann number on velocity. Increasing the Hartmann number strengthens electromagnetic (Lorentz) forces, which suppress fluid

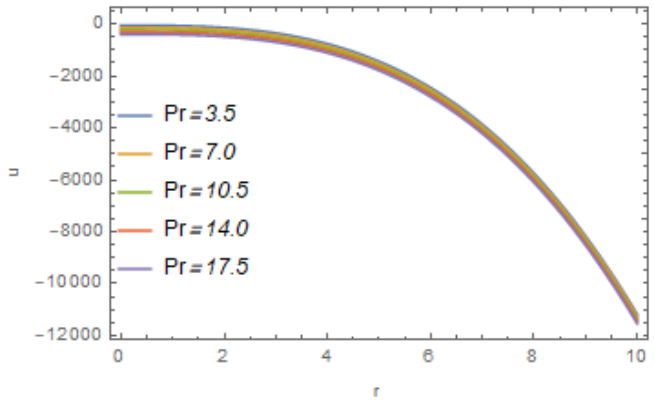


**Figure 11.** Velocity profile u against boundary layer r for varying Prandtl number (Pr).

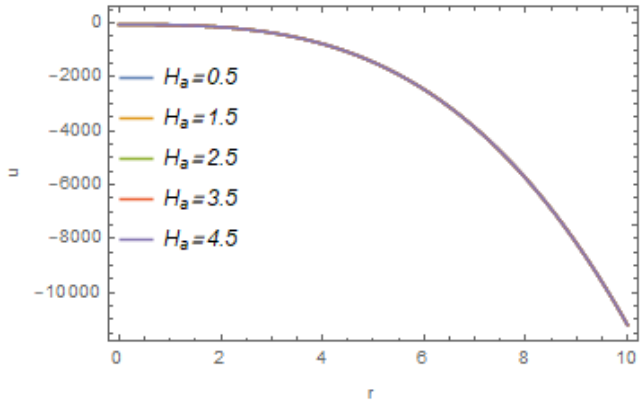


**Figure 12.** Velocity profile u against boundary layer r for varying Magnetic Hartmann number $(H_a)$.

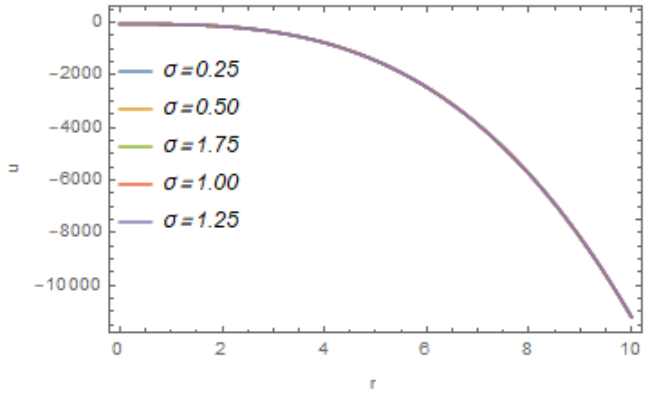


**Figure 13.** Velocity profile u against boundary layer r for varying Electroconductivity parameter $(\sigma)$.

motion. This results in reduced velocity and enhanced flow stability. Lower values allow greater fluid movement due to weaker magnetic influence. The results highlight magnetic field control in EMHD systems. This result agreed with the

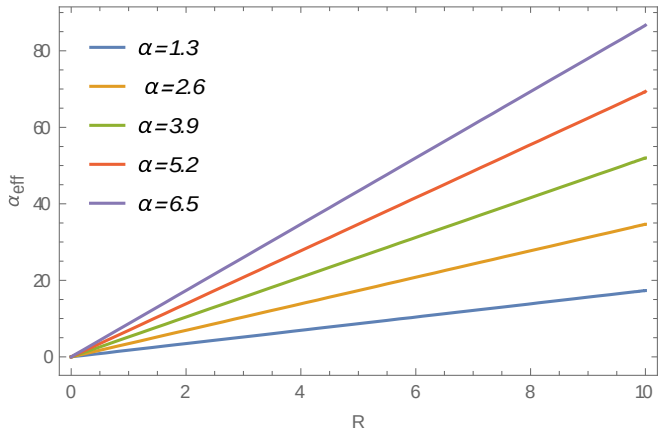


**Figure 14.** Effective Thermal Diffusivity profile $\alpha_{eff}$ against Radiation (R).

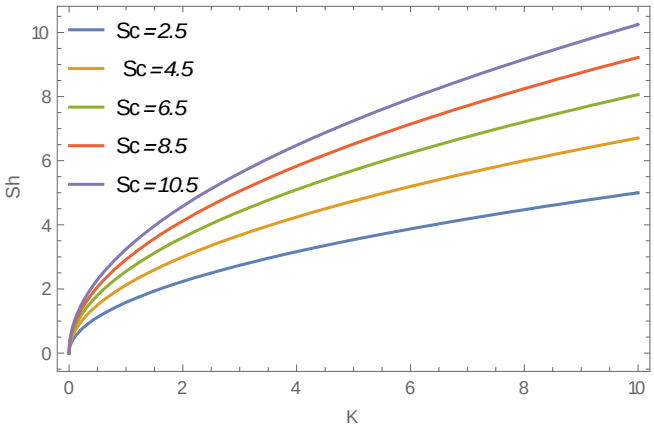


**Figure 15.** Sherwood profile (Sh) against Chemical reaction (K).

findings of Majidi Zar *et al*. (2024).

Figure 13 shows the influence of electrical conductivity on the velocity profile. Higher conductivity enhances electromagnetic interactions, modifying flow behaviour and improving controllability. This result is in agreement with the findings of Albuquerque *et al*. (2024). It acts as a key parameter in regulating fluid motion and stability. Lower conductivity reduces this effect. This is important for EMHD-based material processing.

Figure 14 showcased the variation of effective thermal diffusivity $\alpha_{\text{eff}}$ with radiation parameter (R). Increasing R enhances radiative heat flux, leading to higher $\alpha_{\text{eff}}$. This promotes stronger energy transport and thickens the thermal boundary layer. Heat penetrates deeper into the fluid domain under strong radiation. This is beneficial for thermal treatment applications. The outcome is in agreement with the work of Muhammad *et al*. (2024)

Figure 15 shows the effect of the chemical reaction parameter (K) on the Sherwood number (Sh). Increasing K reduces Sh due to intensified species consumption near

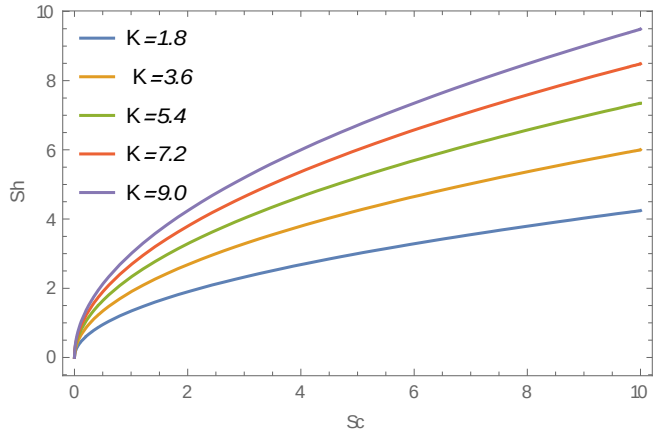


**Figure 16.** Sherwood profile (Sh) against Schmidt number (Sc)

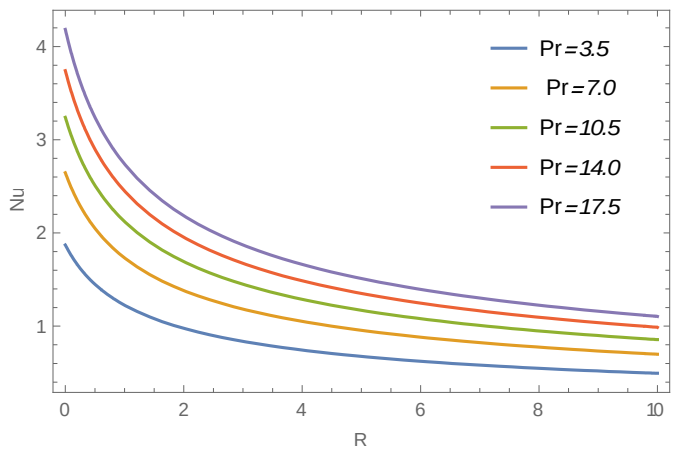


**Figure 17.** Nusselt number (Nu) against Radiation parameter (R).

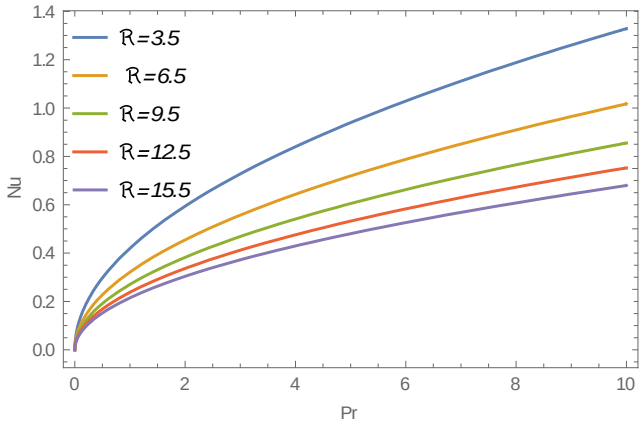


**Figure 18.** Nusselt number (Nu) against Prandtl parameter (Pr).

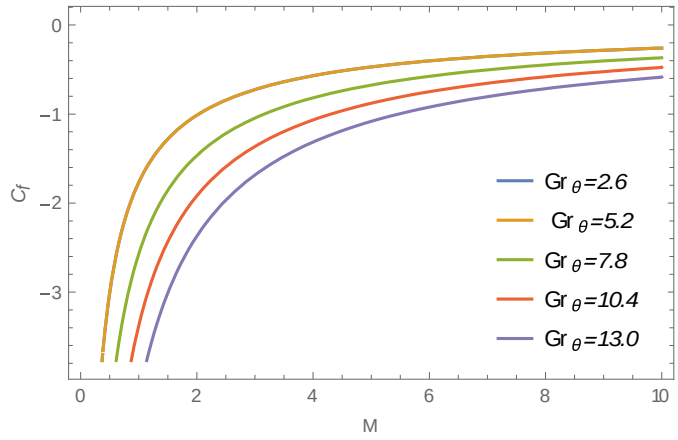


**Figure 19.** Skin friction ($C_f$) against Grashof number in term of temperature $Gr_\theta$.

important for reactive transport processes. This demonstration is in agreement with the work of Nascimento *et al*. (2024).

Figure 16 indicates the variation of Schmidt number (Sc) on Sherwood number (Sh). Higher Sc increases Sh due to reduced mass diffusivity and steeper concentration gradients. This enhances surface mass transfer rates. Lower Sc produces weaker gradients and reduced transfer. The results confirm the role of diffusivity in species transport in agreement with the work of Kayalvizhi and Vijaye (2022).

Figure 17 presents the effect of the radiation parameter (R) on the Nusselt number (Nu). Increasing R enhances heat transfer by strengthening temperature gradients near the surface. This leads to higher Nu values. Radiative the surface. This weakens the concentration gradient responsible for mass transfer. Consequently, diffusion rates decrease within the boundary layer. The result is effects significantly improve thermal performance in agreement with the work of Madkhali *et al.* (2021). The results support the use of r adiation in high-temperature systems.

Figure 18 indicates the variation of Prandtl number (Pr) on Nusselt number (Nu). Higher Pr increases Nu due to reduced thermal diffusivity and sharper temperature gradients. This enhances surface heat transfer efficiency. Lower Pr weakens the thermal gradient and reduces Nu. The findings are relevant for high-viscosity fluid applications and the outcome is in agreement with the work of Sandeep *et al*. (2024).

Figure 19 illustrates the effect of thermal Grashof number $Gr_\theta$ on skin friction coefficient $C_f$. Increasing $Gr_\theta$strengthens buoyancy forces, leading to higher surface shear stress. This enhances momentum transport near the wall. Lower values reduce flow acceleration and shear. The results are important for drag control which is in agreement with the work of Preetham and (2024).

Figure 20 presents the variation of solutal Grashof number $Gr_\phi$on skin friction coefficient $C_f$i. Increasing $Gr_\phi$enhances concentration-induced buoyancy, raising shear stress at the surface. This leads to stronger velocity

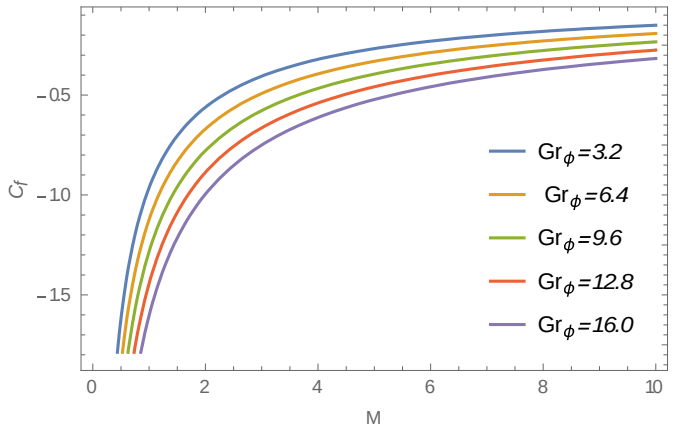


**Figure 20.** Skin friction ($C_f$) against Grashof number in term of concentration $Gr_\phi$.

gradients. Lower values reduce this effect. The findings are significant for mass-transfer-driven flows in line with the work of Muzara and Shateyi (2023).

## Conclusion

In this study, a Hankel-transform-based optimisation framework has been successfully applied to analyse electromagnetohydrodynamic (EMHD) fluid flow over a cylindrical surface, a configuration highly relevant to modern advanced material processing technologies. The cylindrical geometry introduces strong radial interactions, and the application of the zero-order Hankel transform effectively captures these effects by transforming the governing equations into analytically tractable forms. The results reveal that electromagnetic forces play a dominant role in regulating momentum and thermal transport, where increased electromagnetic interaction induces Lorentz damping, thereby suppressing velocity profiles while modifying the temperature field.

The Hankel-based spectral approach demonstrates high computational efficiency and mathematical robustness, offering accurate closed-form solutions in terms of Bessel functions. The parametric optimisation carried out in this work provides critical insights into achieving enhanced thermal uniformity and reduced hydrodynamic resistance in cylindrical processing systems. These findings are particularly valuable for improving operational efficiency in applications such as coating, extrusion, and thermal treatment processes.

Future research may extend this analytical framework to more complex systems, including hybrid nanofluids, transient EMHD flows, and three-dimensional cylindrical geometries, alongside experimental validation for industrial applicability. Overall, the influence of key dimensionless parameters—such as the electromagnetic interaction parameter, Prandtl number, Schmidt number, and thermal radiation parameter—has been comprehensively established, leading to the following major observations:

1. Hankel-based optimisation provides an efficient and accurate analytical tool for controlling EMHD fluid flow over cylindrical surfaces in advanced material processing systems.
2. The velocity and temperature distributions are strongly influenced by electromagnetic interaction, Prandtl number, Schmidt number, and thermal radiation effects.
3. Increasing electromagnetic interaction enhances Lorentz forces, leading to reduced fluid velocity and a thinner momentum boundary layer.
4. Thermal radiation significantly increases radial heat penetration, thereby thickening the thermal boundary layer and improving heat distribution.
5. The study confirms that appropriate tuning of electromagnetic and transport parameters can effectively optimise heat and mass transfer performance in cylindrical manufacturing processes.

## CONFLICT OF INTEREST

The authors declare that they have no conflict of interest.

## REFERENCES

Abbas, W., Megahed, A. M., Emam, M. S., & Sadek, H. M. (2023). MHD dissipative Powell-Eyring fluid flow due to a stretching sheet with convective boundary conditions and slip velocity. *Scientific Reports*, *13*(1), 15674.

Adetoye Solomon, O., Alalibo, N., Micheal, O., & Chijioke Alloysius, E. (2025). Energy Transfer on Magnetohydrodynamic Silver Nanofluid Flow Past a Cylindrical Enclosure. *Journal of Nanofluids*, *14*(5), 639-648.

Ahmad, H., Ozsahin, D. U., Farooq, U., Fahmy, M. A., Albalwi, M. D., & Abu-Zinadah, H. (2023). Comparative analysis of new approximate analytical method and Mohand variational transform method for the solution of wave-like equations with variable coefficients. *Results in Physics*, *51*, 106623.

Albuquerque, L. A. V. D., Villela, M. F. D. S., & Mariano, F. P. (2024). Numerical Simulation of Flows Using the Fourier Pseudospectral Method and the Immersed Boundary Method. *Axioms*, *13*(4), 228.

Alatyar, A. M., Berrouk, A. S., Alshehhi, M. S., Saeed, M., Hassan-Beck, H., & Nandakumar, K. (2023). Design optimization of a rotating packed bed based on dry hydraulic performance. *Alexandria Engineering Journal*, *70*, 475-493.

Aljaloud, A. S., Mumtaz, M. A., Rehman, S., & Ajmal, F. (2025). Machine learning data drive simulation for dual diffusive flow of stratified Maxwell fluid using Cattaneo-Christov heat flux and Darcy-Forchheimer model. *Results in Chemistry*, *20*, 103016.

Alsharif, A. M., Kumar, R., & Singh, S. (2024). Heat and mass transfer analysis of MHD nanofluid flow over a stretching surface with chemical reaction effects. *Journal of Molecular Liquids, 399*, 123456.

Chiba, S. Y., Yuki, K., Hashizume, H., Toda, S., & Sagara, A.

(2006). Numerical research on heat transfer enhancement for high Prandtl-number fluid. *Fusion engineering and design*, *81*(1-7), 513-517.

Gupta, R., Albidah, A. B., Noor, N. F. M., & Khan, I. (2025). Application of DTM to heat source/sink in squeezing flow of iron oxide polymer nanofluid between electromagnetic surfaces. *Case Studies in Thermal Engineering*, *66*, 105735.

Kayalvizhi, J., & Vijaya Kumar, A. G. (2022). Entropy analysis of EMHD hybrid nanofluid stagnation point flow over a porous stretching sheet with melting heat transfer in the presence of thermal radiation. *Energies*, *15*(21), 8317.

Khader, M. M., Babatin, M. M., & Megahed, A. M. (2023). Numerical simulation by using the spectral collocation method for Williamson nanofluid flow over an exponentially stretching sheet with slip velocity. *Journal of Nonlinear Mathematical Physics*, *30*(3), 1134-1152.

Madkhali, H. A., Nawaz, M., Alharbi, S. O., & Elmasry, Y. (2021). An enhancement of energy transport and mass in hybrid nanofluid under magnetic field and temperature and mass concentration gradients. *Case Studies in Thermal Engineering*, *27*, 101182.

Majidi Zar, P., Shateri, A., Jalili, P., Al-Yarimi, F. A., Jalili, B., Ganji, D. D., & Ben Khedher, N. (2025). Radiative effects on 2D unsteady MHD Al2O3-water nanofluid flow between squeezing plates: A comparative study using AGM and HPM in Python. *ZAMM-Journal of Applied Mathematics and Mechanics/Zeitschrift für Angewandte Mathematik und Mechanik*, *105*(2), e202400546.

Mburu, Z. M., Ogutu, S. A., Mondal, S., & Sibanda, P. (2024). Entropy production in unsteady MHD double diffusive and chemically reactive nanofluid flow past a rotating permeable plate using overlapping grid spectral collocation technique. *International Journal of Ambient Energy*, *45*(1), 2280743.

Muhammad, K., Ahmed, B., Sharaf, M., Afikuzzaman, M., & Az-Zo'bi, E. A. (2024). Multiscale tribology analysis of MHD hybrid nanofluid flow over a curved stretching surface. *Nanoscale Advances*, *6*(3), 855-866.

Muzara, H., & Shateyi, S. (2023). Magnetohydrodynamics Williamson nanofluid flow over an exponentially stretching surface with a chemical reaction and thermal radiation. *Mathematics*, *11*(12), 2740.

Nascimento, A. A., Mariano, F. P., da Silveira Neto, A., & Padilla, E. L. M. (2024). Coupling of the immersed boundary and Fourier pseudo-spectral methods applied to solve fluid–structure interaction problems. *Journal of the Brazilian Society of Mechanical Sciences and Engineering*, *46*(4), 213.

Ojo, A. S, Egbo, C. A. & Nwabuzor, P. O. (2026). Analysis of heat transfer models of electromagnetohy drodynamic potassium dichromate ($K_2Cr_2O_7$) nanofluid flow past through the cylindrical coordinate. *Applied Journal of Physical Science, 7(1),* 19-33.

Ojo, A. S., & Egbo, C. A. (2025). Effect of radiation and chemical reaction on ozone layer healings. *Open Journal of Physical Science, 6(*2), 1-13.

Ojo, A. S., Alalibo, N. T., & Onyeaju, M. C. (2025). Numerical analysis of energy transfer on magnetohydrodynamic silver nanofluid flow in cylindrical coordinate. *Open Journal of Physical Science*, *6*(1), 63-82.

Ojo, A. S., Nwabuzor, P. O., Egbo, C. A., & Umoh, E. S. (2026). The Application of Homotopy Perturbation Method in Newtonian Fluids. *Fluid Mechanics*, *11*(1), 1-11.

Preetham, M. P., & Kumbinarasaiah, S. (2024). A numerical study of two-phase nanofluid MHD boundary layer flow with heat absorption or generation and chemical reaction over an exponentially stretching sheet by Haar wavelet method. *Numerical Heat Transfer, Part B: Fundamentals*, *85*(6), 706-735.

Sandeep, A. M., Kumar, P., & Malik, P. S. (2025). Insights into inclined MHD hybrid nanofluid flow over a stretching cylinder with nonlinear radiation and heat flux: A symmetric numerical simulation. *Symmetry*, *17*(11), 1809.

Uda, N., Miyazawa, A., Inoue, S., Yamaoka, N., Horiike, H., & Miyazaki, K. (2001). Forced convection heat transfer and temperature fluctuations of lithium under transverse magnetic fields. *Journal of Nuclear Science and Technology*, *38*(11), 936-943.

Uda, N., Yamaoka, N., Horiike, H., & Miyazaki, K. (2002). Heat transfer enhancement in lithium annular flow under transverse magnetic field. *Energy conversion and management*, *43*(3), 441-447.